1 A higher-order bounded discretization scheme

Baojun Song and Ryo S. Amano
University of Wisconsin–Milwaukee, Milwaukee, WI, USA

Abstract

This chapter presents an overview of the higher-order scheme and introduces a new higher-order bounded scheme, weighted-average coefficient ensuring boundedness (WACEB), for approximating the convective fluxes in solving transport equations with the finite-volume difference method. The weighted-average formulation is used for interpolating the variables at cell faces, and the weighted-average coefficient is determined from normalized variable formulation and total variation diminishing (TVD) constraints to ensure the boundedness of solutions. The new scheme is tested by solving three problems: (1) a pure convection of a box-shaped step profile in an oblique velocity field, (2) a sudden expansion of an oblique velocity field in a cavity, and (3) a laminar flow over a fence. The results obtained by the present WACEB are compared with the upwind and QUICK schemes and show that this scheme has at least the second-order accuracy while ensuring boundedness of solutions. Moreover, it is demonstrated that this scheme produces results that better agree with the experimental data in comparison with other schemes.

Keywords: Finite-volume method, Higher-order scheme

1.1 Introduction

The approximation of the convection fluxes in the transport equations has a decisive influence on the overall accuracy of any numerical solution for fluid flow and heat transfer. Although convection is represented by a simple first-order derivative, its numerical representation remains one of the central issues in CFD. The classic first-order schemes such as upwind, hybrid, and power-law are unconditionally bounded, but tend to misrepresent the diffusion transport process through the addition of numerical or "false" diffusion arising from flow-to-grid skewness. Higher-order schemes, such as the second-order upwind [1] and the third-order upwind (QUICK) [2], offer a route to improve accuracy of the computations. However, they all suffer from the boundedness problem; that is, the solutions may display unphysical

WIT Transactions on State of the Art in Science and Engineering, Vol 41, © 2010 WIT Press
www.witpress.com, ISSN 1755-8336 (on-line)
doi:10.2495/978-1-84564-144-3/01

oscillations in regions of steep gradients, which can be sufficiently serious to cause numerical instability.

During the past two decades, efforts have been made to derive higher resolution and bounded schemes. In 1988, Zhu and Leschziner proposed a local oscillation-damping algorithm (LODA) [3]. Since the LODA scheme introduces the contribution of the upwind scheme, the second-order diffusion is introduced into those regions where QUICK displays unbounded behavior. In 1988, Leonard [4] developed a normalized variable formulation and presented a high-resolution bounded scheme named SHARP (simple high-accuracy resolution program). Gaskell and Lau [5] developed a scheme called SMART (sharp and monotonic algorithm for realistic transport), which employs a curvature-compensated convective transport approximation and a piecewise linear normalized variable formulation. However, numerical testing [6] shows that both SMART and SHARP need an underrelaxation treatment at each of the control volume cell faces in order to suppress the oscillatory convergence behavior. This drawback leads to an increase in the computer storage requirement, especially for three-dimensional flow calculation. In 1991, Zhu [7] proposed a hybrid linear/parabolic approximation (HLPA) scheme. However, this method has only the second-order accuracy.

In the present study, a weighted-averaged formulation is employed to interpolate variables at cell faces and the weighted-average coefficient is determined based on the normalized variable formulation and total variation diminishing (TVD) constraints. Three test cases are examined: a pure convection of a box-shaped step profile in an oblique velocity field, a sudden expansion of an oblique velocity field in a cavity, and laminar flow over a fence. Computations are performed on a generalized curvilinear coordinate system. The schemes are implemented in a deferred correction approach. The computed results are compared with those obtained using QUICK and upwind schemes and available experimental data.

In CFD research, there are three major categories to be considered for flow studies in turbines:

1. *Mathematical models* – the physical behaviors that are to be predicted totally depend on mathematical models. The choice of mathematical models should be carefully made, such as inviscid or viscous analysis, turbulence models, inclusion of buoyancy, rotation, Coriolis effects, density variation, etc.
2. *Numerical models* – selection of a numerical technique is very important to judge whether or not the models can be effectively and accurately solved. Factors that need to be reviewed for computations include the order of accuracy, treatment of artificial viscosity, consideration of boundedness of the scheme, etc.
3. *Coordinate systems* – the type and structure of the grid (structured or unstructured grids) directly affect the robustness of the solution and accuracy.

Numerical studies demand, besides mathematical representations of the flow motion, a general, flexible, efficient, accurate, and – perhaps most importantly – stable and bounded (free from numerical instability) numerical algorithm for solving a complete set of average equations and turbulence equations. The formulation

Table 1.1. Schemes used in CFD

Scheme	Developers	Order	False diffusion	Boundedness
Upwind	–	1st	High	Unconditionally bounded
Hybrid	Gosman (1977)	1st	High	Unconditionally bounded
Power-law	Patankar (1980)	1st	Medium	Unconditionally bounded
Second-order upwind	Price et al. (1966)	2nd	Low	Unbounded
QUICK	Leonard (1979)	3rd	Low	Unbounded
LODA	Zhu–Leschziner (1988)	2nd	Low	Conditionally bounded
SHARP	Leonard (1988)	2nd	Low	Conditionally bounded
SMART	Gaskell–Lau (1988)	2nd	Low	Conditionally bounded
WACEB	Song et al. (1999)	2nd	Low	Unconditionally bounded

of the discretization scheme of convection fluxes may be one of the major tasks to meet such demands.

As for the numerical method, the classic first-order schemes such as upwind, hybrid, and power-law [8] are unconditionally bounded (solutions do not suffer from over/undershoot), but tend to misrepresent the transport process through addition of numerical diffusion arising from flow-to-grid skewness. These are the schemes that most of the commercial codes employ. In some applications, small overshoots and undershoots may be tolerable. However, under other circumstances, the nonlinear processes of turbulence diffusion will feed back and amplify these over/undershoots, and may lead to divergence of a solution. During the past decade, efforts have been made to derive high-resolution and bounded schemes. LODA, SHARP, and SMART all display unbounded behavior, which leads to an increase in the computer storage requirement, especially for three-dimensional flow calculations. Therefore, the traditional method for simulating turbulent flows is the hybrid (upwind/central differencing) scheme, and the upwind is used for turbulence equations such as kinetic energy equation, dissipation rate equation, and Reynolds stress equations. Since it has a poor track record, one should always be suspicious of the first-order upwind scheme.

1.2 Numerical Formulation

1.2.1 Governing equations

The conservation equations governing incompressible steady flow problems are expressed in the following general form:

$$\mathrm{div}[\rho\vec{V}\Phi - \Gamma_\Phi \mathrm{grad}(\Phi)] = S_\Phi \tag{1}$$

where Φ is any transport variable, $\vec{V}$ the velocity vector, ρ the density of the fluid, Γ^Φ the diffusive coefficient, and S_Φ is the source term of variable Φ.

With ξ, η, and ζ representing the general curvilinear coordinates in three-dimensional framework, the transport equation (1) can be expressed as:

$$\frac{1}{J}\left[\frac{\partial \rho U\Phi}{\partial\xi} + \frac{\partial \rho V\Phi}{\partial\eta} + \frac{\partial \rho W\Phi}{\partial\zeta}\right] = \frac{1}{J}\frac{\partial}{\partial\xi}\left[\frac{\Gamma_\Phi}{J}(q_{11}\Phi_\xi)\right] + \frac{1}{J}\frac{\partial}{\partial\eta}\left[\frac{\Gamma_\Phi}{J}(q_{22}\Phi_\eta)\right] + \frac{1}{J}\frac{\partial}{\partial\zeta}\left[\frac{\Gamma_\Phi}{J}(q_{33}\Phi_\zeta)\right] + S^{\mathrm{CD}} + S_\Phi(\xi,\eta,\zeta) \tag{2}$$

where U, V, and W are contravariant velocities defined as follows:

$$U = j_{11}u + j_{21}v + j_{31}w \tag{3a}$$

$$V = j_{12}u + j_{22}v + j_{32}w \tag{3b}$$

$$W = j_{13}u + j_{23}v + j_{33}w \tag{3c}$$

J is the Jacobian coefficient, q_{ij} and j_{ij} ($i = 1-3$ and $j = 1-3$) are the transformation coefficients (refer to the appendix), and S^{CD} is the cross-diffusion term (refer to the appendix).

1.2.2 Discretization

The computational domain is uniformly divided into hexahedral control volumes, and the discretization of transport equation (2) is performed in the computational domain following the finite-volume method.

Integrating equation (2) over a control volume as shown in Figure 1.1 and applying the *Gauss Divergence Theorem* in conjunction with central difference for diffusion, we have:

$$F_\mathrm{e} - F_\mathrm{w} + F_\mathrm{n} - F_\mathrm{s} + F_\mathrm{t} - F_\mathrm{b} = S_\Phi \Delta V + S^{\mathrm{CD}}\Delta V \tag{4}$$

where F_f represents the total fluxes of Φ across the cell face f (f = e, w, b, s, b, t).

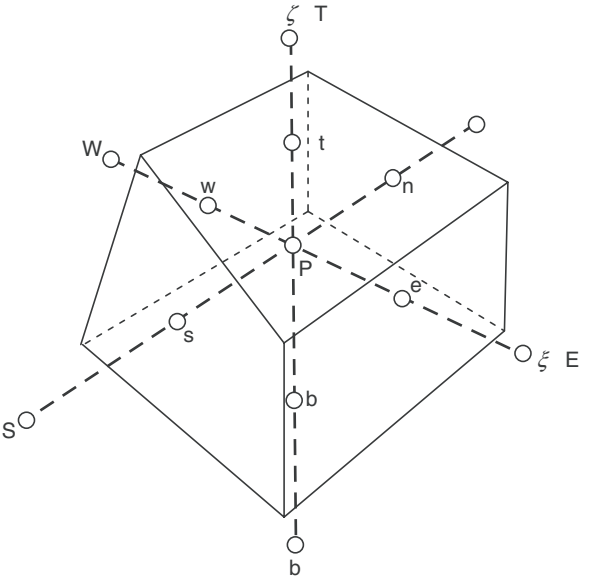

Figure 1.1. A typical control volume.

Taking the east face as an example, the total fluxes across it can be written as:

$$F_e = (\rho U \Phi)_e - \left(\frac{\Gamma^\Phi}{J} J_{11}\right)_e (\Phi_E - \Phi_P) \tag{5}$$

In the above equation, the cell face values of Φ can be approximated with different schemes.

For the first-order upwind scheme, the cell face value is expressed as:

$$\begin{aligned} \Phi_e &= \Phi_P \qquad \text{if } U_e > 0 \\ \Phi_e &= \Phi_E \qquad \text{if } U_e < 0 \end{aligned} \tag{6}$$

Substituting equations (5) and (6) into equation (4), we have:

$$A_P \Phi_P = \sum_{i=E,W,N,S,T,B} A_i \Phi_i + S_C \tag{7}$$

where subscript i denotes neighboring grid points, A_P and A_i the coefficients relating to the convection and diffusion, and S_c is the source term.

1.2.3 Higher-order schemes

The approximation of convection has a decisive influence on the overall accuracy of the numerical simulations for a fluid flow. The first-order schemes such as upwind, hybrid, and power-law all introduce the second-order derivatives that then lead to falsely diffusive simulated results. Therefore, the higher-order schemes have

to be used to increase the accuracy of the solution. Generally, with uniform grid spacing, the higher-order interpolation schemes can be written in the following weighted-average form:

$$\Phi_e = \underline{\Phi_P} + \frac{1}{4}[(1-\kappa)\Delta_e^- + (1+\kappa)\Delta_e] \quad \text{if } U_e > 0$$
$$\Phi_e = \underline{\Phi_E} - \frac{1}{4}[(1-\kappa)\Delta_e^+ + (1+\kappa)\Delta_e] \quad \text{if } U_e < 0 \tag{8}$$

where $\Delta_e^- = \Phi_P - \Phi_W$, $\Delta_e = \Phi_E - \Phi_P$, $\Delta_e^+ = \Phi_{EE} - \Phi_E$ and κ is the weighted-average coefficient. In equation (8), the underlined terms represent the fragments of the first-order upwind scheme. Therefore, the higher-order schemes can be implemented in a deferred correction approach proposed by Khosla and Rubin [9]; that is,

$$\Phi_f^{n+1} = \Phi_f^{UP,n+1} + (\Phi_f^{HO,n} - \Phi_f^{UP,n}) \tag{9}$$

where n indicates the iteration level, and UP and HO refer to the upwind and higher-order schemes, respectively. The convective fluxes calculated by the upwind schemes are combined with the diffusion term to form the main coefficients of the difference equation, while those resulting from the deferred correction terms are collected into the source term, say, S^{DC}. Such a treatment leads to a diagonally dominant coefficient matrix and enables a higher-order accuracy to be achieved at a converged stage.

With this method, the deferred correction source term, taking east–west direction as an example, is calculated by:

$$S^{DC} = \frac{1}{4}\left\{U_e^+ U_e[(1+\kappa)\Delta_e + (1-\kappa)\Delta_e^-] - U_e^- U_e[(1+\kappa)\Delta_e + (1-\kappa)\Delta_e^+]\right.$$
$$\left. - U_w^+ U_w[(1+\kappa)\Delta_w + (1-\kappa)\Delta_w^-] + U_w^- U_w[(1+\kappa)\Delta_w + (1-\kappa)\Delta_w^+]\right\} \tag{10}$$

where $U_e^{\pm}$ is defined as:

$$U_f^{\pm} = \frac{1 \pm \mathrm{sgn}(U_f)}{2}$$

If κ is fixed at a suitable constant value everywhere, several well-known schemes can be formed.

However, the schemes listed in Table 1 all suffer from boundedness problem; that is, the solutions may display unphysical oscillations in regions of steep gradients, which can be sufficiently serious to lead to numerical instability.

1.2.4 Weighted-average coefficient ensuring boundedness

Based on the variable normalization proposed by Leonard [4], with a three-node stencil as shown in Figure 1.2, we introduce a normalized variable defined as:

$$\tilde{\Phi} = \frac{\Phi - \Phi_U}{\Phi_D - \Phi_U} \tag{11}$$

Table 1.2. Typical interpolation schemes

Expression for Φ_e when $u > 0$	Leading truncation error term
$1/2(3\Phi_P - \Phi_W)$	$3/8\Delta x^3\Phi''$
$1/2(\Phi_E + \Phi_P)$	$1/8\Delta x^2\Phi''$
$1/8(3\Phi_E + 6\Phi_P - \Phi_W)$	$1/16\Delta x^3\Phi'''$
$1/6(2\Phi_E + 5\Phi_P - \Phi_W)$	$-1/24\Delta x^2\Phi''$

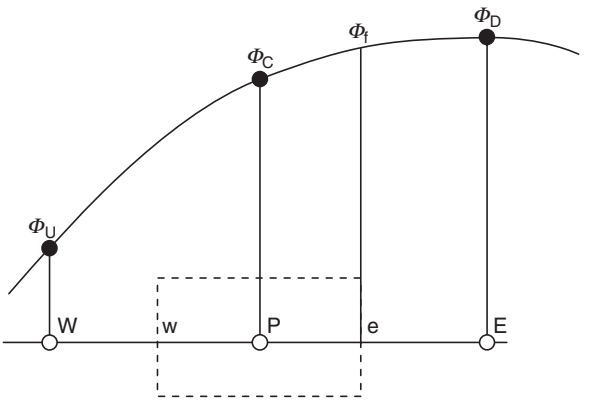

Figure 1.2. Three-node stencil.

where the subscripts U and D represent the upstream and downstream locations, respectively. In the normalized form, the higher-order schemes can be rewritten as:

$$\tilde{\Phi}_f = \tilde{\Phi}_C + \frac{1}{4}[(1+\kappa)(1-\tilde{\Phi}_C) + (1-\kappa)\tilde{\Phi}_C] \tag{12}$$

See Figure 1.2 for notations of the terms. Solving for κ,

$$\kappa = \frac{4\tilde{\Phi}_f - 4\tilde{\Phi}_C - 1}{1 - 2\tilde{\Phi}_C} \tag{13}$$

In order to ensure boundedness, the TVD constraints can be used; that is,

$$\begin{aligned} &\tilde{\Phi}_f \le 1, \tilde{\Phi}_f \le 2\Phi_C, \tilde{\Phi}_f \ge \tilde{\Phi}_C \quad \text{for} \quad 0 < \tilde{\Phi}_C < 1 \\ &\tilde{\Phi}_f = \tilde{\Phi}_C \qquad\qquad\qquad\quad \text{for} \quad \tilde{\Phi}_C \le 0 \quad \text{or} \quad \tilde{\Phi}_C \ge 1 \end{aligned} \tag{14}$$

which correspond to the triangle region shown in Figure 1.3.

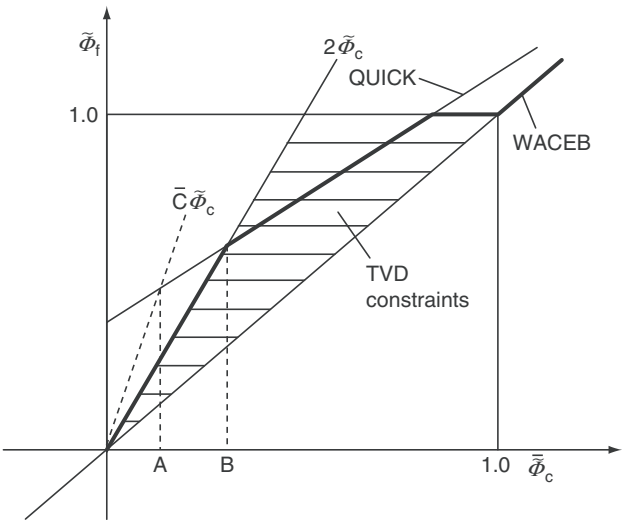

Figure 1.3. Diagrammatic representation of the TVD constraint and WACEB scheme.

The Taylor series expansion shows that the first two leading truncation error terms of the interpolation scheme (7) are $1/4(\kappa - 1/2)\Delta x^2\Phi''$ and $1/8(1-\kappa)\Delta x^3\Phi'''$. Therefore, the scheme has at least the second-order accuracy. The maximum accuracy (third order) can be achieved if κ is set equal to 1/2. Thus, the scheme can be formed in such a way that κ lies as close as possible to 1/2, while satisfying the TVD constraints. Based on this idea, the normalized cell face value can be computed by the following expressions:

$$\tilde{\Phi}_f = \begin{cases} \tilde{\Phi}_C & \tilde{\Phi}_C \notin [0,1] \\ 2\tilde{\Phi}_C & \tilde{\Phi}_C \in [0,0.3) \\ 3/8\,(2\tilde{\Phi}_C + 1) & \tilde{\Phi}_C \in [0.3,5/6] \\ 1 & \tilde{\Phi}_C \in (5/6,1] \end{cases} \tag{15}$$

As shown in Figure 1.3, TVD constraints are overly restrictive according to convection boundedness criterion (CBC). However, the use of a larger multiplying constant will not noticeably increase the accuracy. The reasons are that, first, the constant affects the accuracy only in the range from A to B (see Figure 1.3), and this range varies at most from 0 to 0.3 (if we use constant 3, $A = 0.1666$ and $B = 0.3$). Secondly, even with the smaller constant, the accuracy of the scheme is still second order. Therefore, the present WACEB (weighted-average coefficient ensuring boundedness) scheme employs normalized variable formulation (15) to calculate the weighted-average coefficient to preserve boundedness.

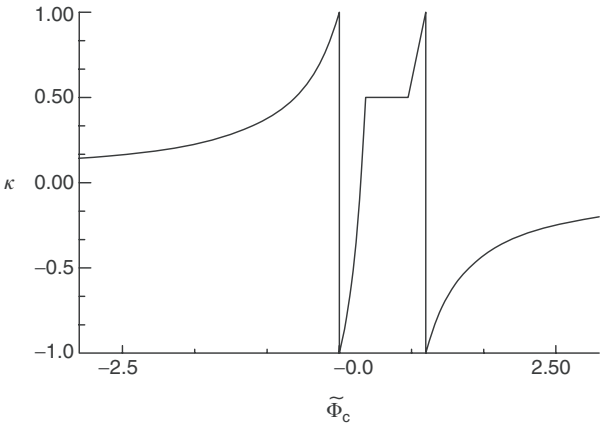

Figure 1.4. The variation in weighted-average coefficient with normalized variable.

From equations (7) and (8), the weighted-average coefficient can be given by:

$$\kappa = \begin{cases} 1/(1-2\tilde{\Phi}_C) & \tilde{\Phi}_C \notin [0,1] \\ (4\tilde{\Phi}_C - 1)/1 - 2\tilde{\Phi}_C & \tilde{\Phi}_C \in [0,0.3) \\ (3-4\tilde{\Phi}_C)/(1-2\tilde{\Phi}_C) & \tilde{\Phi}_C \in [0.3,5/6] \\ 1/2 & \tilde{\Phi}_C \in (5/6,1] \end{cases} \tag{16}$$

The variation in κ with $\tilde{\Phi}_C$ is shown in Figure 1.4. It is easy to see that the present WACEB scheme satisfies convective stability condition [2]. It is necessary to mention that the above algorithm is formulated on the assumption of the constant grid spacing. For nonuniform grids, the weighted-average coefficient will also be the function of the grid spacing aspect ratio.

1.3 Test Problem and Results

The governing transport equations are solved by using the nonstaggered finite-volume method. A special interpolation procedure developed by Rhie and Chow [10] is used to prevent pressure oscillations due to nonstaggered grid arrangement. Pressure and velocity coupling is achieved through the SIMPLE algorithm [8].

It is necessary to mention that QUICK and WACEB schemes all need to employ two upstream nodes for each cell face, which mandates one to involve a value outside the solution domain for a near-boundary control volume. Therefore, the upwind scheme is used for all the control volume adjacent to boundaries.

1.3.1 Pure convection of a box-shaped step profile

The flow configuration shown in Figure 1.5 constitutes a test problem for examining the performance of numerical approximation to convection because of the extremely

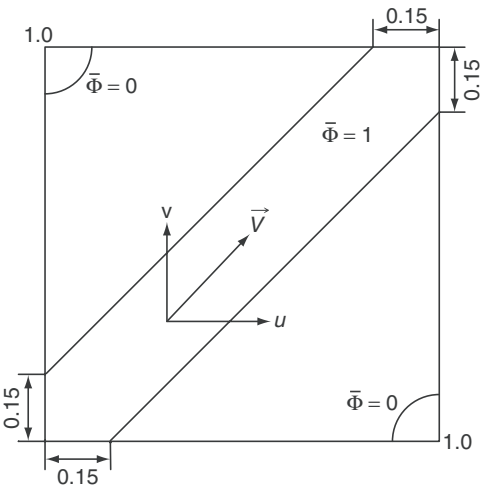

Figure 1.5. Pure convection of a box-shaped step by a uniform velocity field.

sharp gradient in a scalar. This is a linear problem in which the velocity field is prescribed. The calculations are performed with two different uniform meshes, 29×29 and 59×59.

Comparisons of the numerical solutions obtained with the upwind, QUICK, and WACEB schemes are presented in Figure 1.6(a) and (b). It can be seen that the upwind scheme results in a quite falsely diffusive profile for the scalar even with the finer mesh. Although the QUICK scheme reduces such a false diffusion, it produces significant overshoots and undershoots. Unlikely, the WACEB predicts a fairly good steep gradient without introducing any overshoots or undershoots. Therefore, we conclude that the WACEB scheme resolves the boundedness problem while reserving a higher-order accuracy.

1.3.2 Sudden expansion of an oblique velocity field in a cavity

The geometry under consideration is depicted in Figure 1.7. The flow is assumed to be steady and laminar. At the inlet, U-velocity and V-velocity are given a constant value of U_{ref}. The boundary conditions at the outlet are $\partial U/\partial x = 0$ and $\partial V/\partial x = 0$. The calculations are performed on the uniform meshes (59×59). Figure 1.8 shows the comparison of U-velocity along the vertical central lines of the cavity for the Reynolds number 400. It is noticed that the upwind scheme cannot predict the secondary recirculation region well, which should appear near the upper side of the cavity and smears out the steep gradients of the velocity profile near the mainstream. We observe that both the WACEB and QUICK schemes distinctively predict this secondary recirculating region. Furthermore, it is noteworthy to observe that both produce very similar results. The streamline patterns predicted with the three schemes are all shown in Figure 1.9. It is clearly seen, again, that the upwind

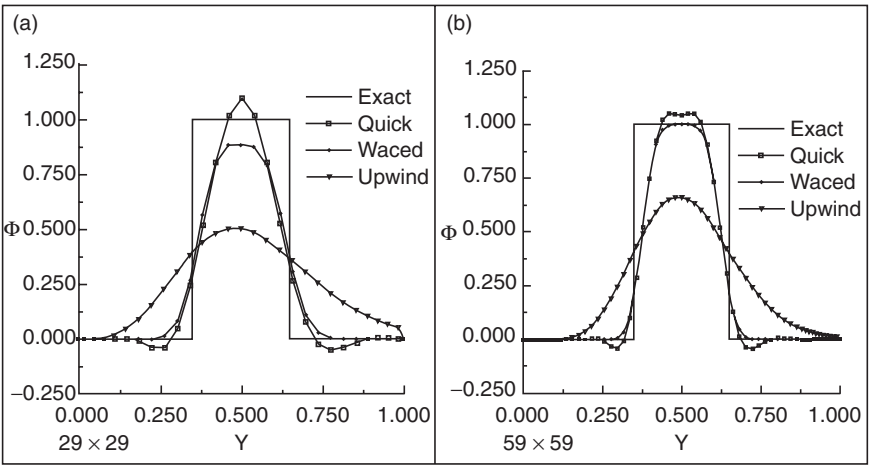

Figure 1.6. Scalar profiles along the center line.

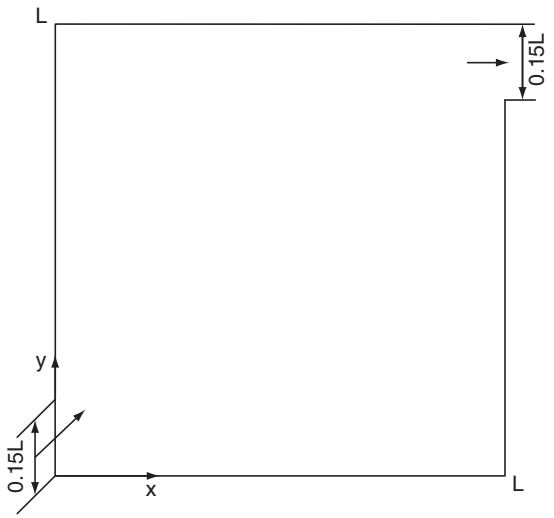

Figure 1.7. Geometry of a cavity.

scheme predicts a much smaller vortex on the upper left side of the cavity and much wider mainstream region than the QUICK and WACEB schemes. The computations were further extended to a higher Reynolds number up to 1,000. At this Reynolds number, the QUICK scheme produces a "wiggle solution." Figure 1.10 shows streamline patterns predicted with the WACEB and upwind schemes. These two schemes give very different flow patterns; with the increase in the Reynolds number, the convection is enhanced and diffusion is suppressed and then the "dead water regions" should have less effect on the mainstream region. The results with

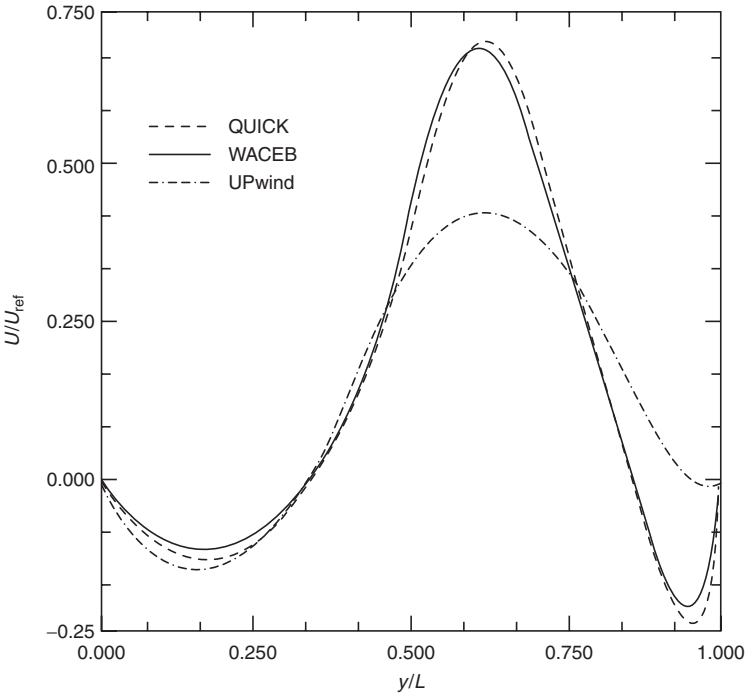

Figure 1.8. U-velocity profile along the vertical center line of the domain (Re = 400).

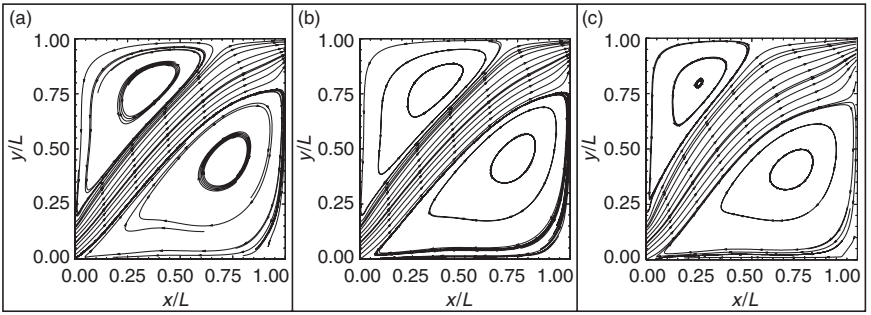

Figure 1.9. Streamlines for sudden expansion of an oblique velocity field (Re = 400): (a) QUICK; (b) WACEB; (c) upwind.

the WACEB scheme clearly show this trend. It is also noted that the WACEB scheme produces two additional vortices at the two corners of the cavity. However, the upwind scheme predicts only a very small additional vortex at the lower right corner and fails to capture the additional vortex at the upper left corner.

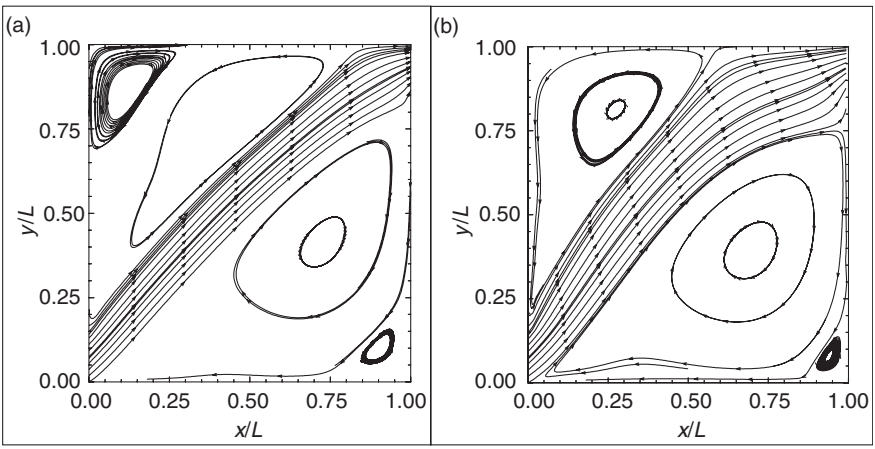

Figure 1.10. Streamlines for sudden expansion of an oblique velocity field (Re = 1,000): (a) WACEB; (b) upwind.

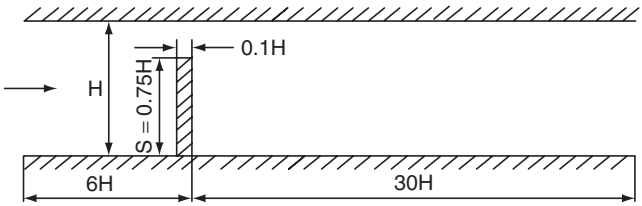

Figure 1.11. Geometry of flow over a fence.

From the above discussions, it is concluded that the solution with the WACEB scheme is comparable to that with the QUICK scheme. Even under highly convective conditions in which the unbounded QUICK scheme may produce "wiggle solutions," the bounded WACEB scheme still produces a reasonable solution.

1.3.3 Two-dimensional laminar flow over a fence

A two-dimensional laminar flow over a fence (see Figure 1.11) with the Reynolds number based on the height of the fence, the mean axial velocity of 82.5, and the blockage ratio (s/H) of 0.75 is a benchmark case study. The boundary conditions at the inlet are prescribed as a parabolic profile for the axial velocity U and zero for the cross-flow velocity V. At the outlet, the boundary conditions are given as $\partial U/\partial x = 0$ and $\partial V/\partial x = 0$. The present study shows that the grid-independence results can be achieved with 150×78 uniform meshes for all the schemes.

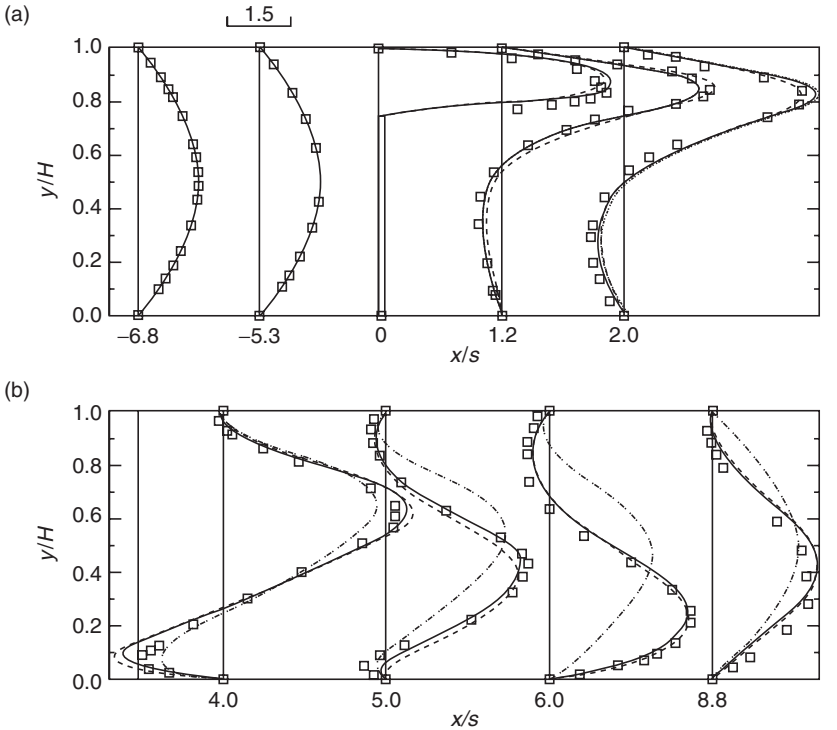

Figure 1.12. Comparison between prediction and measurement for flow over the fence (Re = 82.5) (square symbol, experimental data; solid line, WACEB; dashed line, QUICK; dash–dot line, upwind)

Figure 1.12 presents the axial velocity profiles at different locations (x/s) measured [11] and calculated with the QUICK, WACEB, and upwind schemes. We can observe that when x/s is less than 2, the results with the three schemes are nearly identical and are in good agreement with experimental data. However, when x/s is larger than 2, where the second separated flow on the top wall appears, the upwind scheme predicts very poor results and the QUICK and WACEB schemes give very satisfactory results in comparison with the experimental data [11]. These results verify the conclusion drawn from previous section.

1.4 Conclusions

By using normalized variable formulation and TVD constraints, the WACEB of the solution is determined and then a bounded scheme is presented in this chapter. This new scheme is tested for four different flow applications including a linear convection transport of a scalar, a sudden expansion of an oblique flow field, and a

laminar flow over a fence. The numerical tests show that the new WACEB scheme retains the ability of the QUICK to reduce the numerical diffusion without introducing any overshoots or undershoots. The scheme is very easy to implement, stable, and free of convergence oscillation and does not need to incorporate any under-relaxation treatment for weighted-average coefficient calculation.

Appendix

The cross-diffusion source term in equation (2) is defined as follows:

$$S^{\mathrm{CD}} = \frac{1}{J}\frac{\partial}{\partial\xi}\left(\frac{\Gamma_\Phi}{J}(q_{21}\Phi_\eta + q_{31}\Phi_\zeta)\right) + \frac{1}{J}\frac{\partial}{\partial\eta}\left(\frac{\Gamma_\Phi}{J}(q_{12}\Phi_\xi + q_{32}\Phi_\zeta)\right) + \frac{1}{J}\frac{\partial}{\partial\zeta}\left(\frac{\Gamma_\Phi}{J}(q_{13}\Phi_\xi + q_{23}\Phi_\eta)\right)$$

The transformation coefficients are defined as follows:

$$j_{11} = \frac{\partial y}{\partial\eta}\frac{\partial z}{\partial\zeta} - \frac{\partial y}{\partial\zeta}\frac{\partial z}{\partial\eta},\ j_{12} = \frac{\partial y}{\partial\zeta}\frac{\partial z}{\partial\xi} - \frac{\partial y}{\partial\xi}\frac{\partial z}{\partial\zeta},\ j_{13} = \frac{\partial y}{\partial\xi}\frac{\partial z}{\partial\eta} - \frac{\partial y}{\partial\eta}\frac{\partial z}{\partial\xi},$$
$$j_{21} = \frac{\partial x}{\partial\zeta}\frac{\partial z}{\partial\eta} - \frac{\partial x}{\partial\eta}\frac{\partial z}{\partial\zeta},\ j_{22} = \frac{\partial x}{\partial\xi}\frac{\partial z}{\partial\zeta} - \frac{\partial x}{\partial\zeta}\frac{\partial z}{\partial\xi},\ j_{23} = \frac{\partial x}{\partial\eta}\frac{\partial z}{\partial\xi} - \frac{\partial x}{\partial\xi}\frac{\partial z}{\partial\eta},$$
$$j_{31} = \frac{\partial x}{\partial\eta}\frac{\partial y}{\partial\zeta} - \frac{\partial x}{\partial\zeta}\frac{\partial y}{\partial\eta},\ j_{32} = \frac{\partial x}{\partial\zeta}\frac{\partial y}{\partial\xi} - \frac{\partial x}{\partial\xi}\frac{\partial y}{\partial\zeta},\ j_{33} = \frac{\partial x}{\partial\xi}\frac{\partial y}{\partial\eta} - \frac{\partial x}{\partial\eta}\frac{\partial y}{\partial\xi}$$

and

$$q_{ij} = \sum_{k=1}^{3} j_{ki}j_{kj} \quad (i = 1,3,\ j = 1,3)$$

Nomenclature

A	coefficients in equation (7)
F	total fluxes across the cell faces
H	height of channel
J	determinant of Jacobian
j_{ij}, q_{ij} ($i = 1,3$ and $j = 1,3$)	transformation factor
L	length of cavity
Re	Reynolds number
$S_\Phi, S_C, S^{\mathrm{CD}}, S^{\mathrm{DC}}$	source term
s	hight of fence
U, V, W	contravariant velocity components
U_m	mean velocity in the channel
u, v, w	Cartesian velocity components
x, y, z	Cartesian coordinates

Greek Symbols

Γ	diffusion coefficient
κ	weighted-average coefficient
Φ	dependent variable
ξ, η, ζ	generalized curvilinear coordinates

Superscript

HO	term associated with higher-order scheme
UP	term associated with upwind scheme
n	iteration level
$\sim$	normalized value

Subscripts

f (=e, w, n, s, t, b)	value at the cell faces
F (=E, W, N, S, T, B)	value at the nodes

References

[1] Price, H. S. Varga, R. S., and Warren, J. E. Application of oscillation matrices to diffusion-correction equations, *J. Math. Phys.*, 45, pp. 301–311, 1966.
[2] Leonard, B. P. A stable and accurate convective modelling procedure based on quadratic upstream interpolation, *Comput. Methods Appl. Mech. Eng.*, 19, pp. 59–98, 1979.
[3] Zhu, J., and Leschziner, M. A. A local oscillation-damping algorithm for higher-order convection schemes, *Comput. Methods Appl. Mech. Eng.*, 67, pp. 355–366, 1988.
[4] Leonard, B. P. Simple high-accuracy resolution program for convective modelling of discontinuities, *Int. J. Numer. Methods Fluids*, 8, pp. 1291–1318, 1988.
[5] Gaskell, P. H., and Lau, A. K. C. Curvature-compensated convective transport: SMART, a new boundedness preserving transport algorithm, *Int. J. Numer. Methods Fluids*, 8, pp. 617–641, 1988.
[6] Zhu, J. On the higher-order bounded discretization schemes for finite volume computations of incompressible flows, *Comput. Methods Appl. Mech. Eng.*, 98, pp. 345–360, 1992.
[7] Zhu, J. A low-diffusive and oscillation-free convection scheme, *Comm. Appl. Numer. Methods*, 7, pp. 225–232, 1991.
[8] Patankar, S. V. *Numerical Heat Transfer and Fluid Flow*, McGraw-Hill, New York 1980.
[9] Khosla, P. K., and Rubin, S. G. A diagonally dominant second-order accurate implicit scheme, *Comput. Fluids*, 2, pp. 207–209, 1974.
[10] Rhie, C. M., and Chow, W. L. A numerical study of the turbulent flow past an isolated airfoil with trailing edge separation, *AIAA J.*, 21, pp. 1525–1532, 1983.
[11] Carvalho, M. G. Durst, F., and Pereira, J. C. Predictions and measurements of laminar flow over two-dimensional obstacles, *Appl. Math. Model*., 11, pp. 23–34, 1987.